ACS APPLIED MATERIALS & INTERFACES

Research Article

Cite This: ACS Appl. Mater. Interfaces 2018, 10, 14540−14548

www.acsami.org

Electrospun Polyhydroxybutyrate/Poly(ε-caprolactone)/Sol−Gel-Derived Silica Hybrid Scaffolds with Drug Releasing Function for Bone Tissue Engineering Applications

Yaping Ding,[†,‡] Wei Li,[†] Alexandra Correia,[†] Yuyun Yang,[§,∥] Kai Zheng,[§] Dongfei Liu,[†,⊥] Dirk W. Schubert,[‡] Aldo R. Boccaccini,[§] Hélder A. Santos,*[,†,⊥] and Judith A. Roether*[,‡]

[†]Drug Research Program, Division of Pharmaceutical Chemistry and Technology, Faculty of Pharmacy, and [⊥]Helsinki Institute of Life Science (HiLIFE), University of Helsinki, FI-00014 Helsinki, Finland

[‡]Institute of Polymer Materials, University of Erlangen−Nuremberg, Martensstrasse 7, 91058 Erlangen, Germany

[§]Institute of Biomaterials, University of Erlangen−Nuremberg, Cauerstrasse 6, 91058 Erlangen, Germany

[∥]Institute of Corrosion Science and Surface Technology, Harbin Engineering University, Nantong Street 145, 150001 Harbin, China

ABSTRACT: Electrospun hybrid scaffolds are an effective platform to deliver drugs site specifically for the prevention and treatment of diseases in addition to promote tissue regeneration because of the flexibility to load drugs therein. In the present study, electrospun hybrid scaffolds containing antibiotics were developed to support cellular activities and eliminate potential postoperative inflammation and infection. As a model drug, levofloxacin (LFX) was successfully incorporated into pure polyhydroxybutyrate/poly(ε-caprolactone) (PHB/PCL) scaffolds and PHB/PCL/sol−gel-derived silica (SGS) scaffolds. The influence of LFX on the morphology, mechanical performance, chemical structure, drug release profile, and antibacterial effect of the scaffolds was thoroughly and comparatively investigated. MG-63 osteoblast-like cell cultivation on both scaffolds certified that LFX inclusion did not impair the biocompatibility. In addition to the favorable cellular proliferation and differentiation, scaffolds containing both LFX and SGS displayed highly increased mineralization content. Therefore, the present multifunctional hybrid scaffolds are promising in tissue engineering applications.

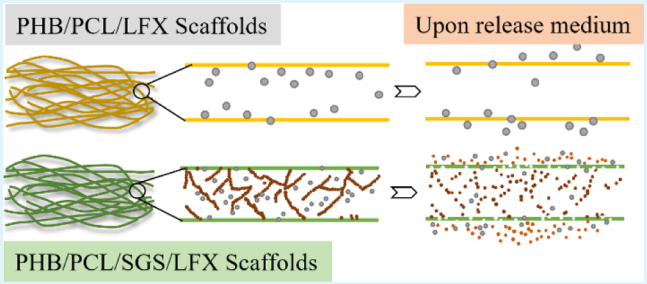

KEYWORDS: *polyhydroxybutyrate, poly(ε-caprolactone), sol−gel silica, hybrid scaffolds, antibacterial*

1. INTRODUCTION

As a simple and versatile technique to generate three-dimensional (3D) and highly porous architectures, consisting of continuous fibers down to nanosize, electrospinning has been applied for various applications such as biomedical, agricultural, energy industries, and so forth.[1−3] Biomedical applications such as tissue engineering and drug delivery are recognized as the most technically relevant among those applications.[3] On the one hand, nonwoven nanofibers fabricated via electrospinning possess highly interconnected pores up to 90% in volume, thus imitating the extracellular matrix (ECM) closely, and can favorably support cell adhesion, proliferation, differentiation, and ultimately tissue regeneration.[4] On the other hand, flexible drug entrapment through direct blending or incorporation of particulate vehicles, high drug loading capacity, and nearly 100% encapsulation efficiency makes the fibrous scaffolds an optimal platform to locally deliver a variety of drugs.[2] Additionally, because of topical administration, the required drug dosage in electrospun fibers can be reduced, leading to less systematic adsorption and reduced side effects.[5,6] These advantages of electrospinning, therefore, make it a promising technique to develop multifunctional scaffolds that meet the diverse requirements in tissue engineering. For instance, in bone tissue engineering, biocompatible and bioactive scaffolds with an antibacterial function are desired because they could greatly reduce the possibility of postoperative inflammation and infection.[7]

Several studies have focused on drug incorporation into polymer scaffolds or ceramic scaffolds.[6,8−10] However, drug incorporation in organic/inorganic hybrids and their drug release behaviors are rarely reported. Aiming for bone tissue engineering, polyhydroxybutyrate/poly(ε-caprolactone) (PHB/PCL)/sol−gel-derived silica (SGS) hybrid scaffolds were successfully fabricated in our previous study and their physiochemical and biocompatibility were thoroughly characterized.[11,12] SGS was able to promote the bioactivity of polymer matrix, and the PHB/PCL/SGS hybrid scaffolds were favorable for osteogenicity.[12] As a widely used antibiotic in clinic, levofloxacin (LFX) is active against a variety of clinical pathogens including both Gram-negative bacteria and Gram-

Received: February 12, 2018
Accepted: April 6, 2018
Published: April 6, 2018

DOI: 10.1021/acsami.8b02656
ACS Appl. Mater. Interfaces 2018, 10, 14540−14548

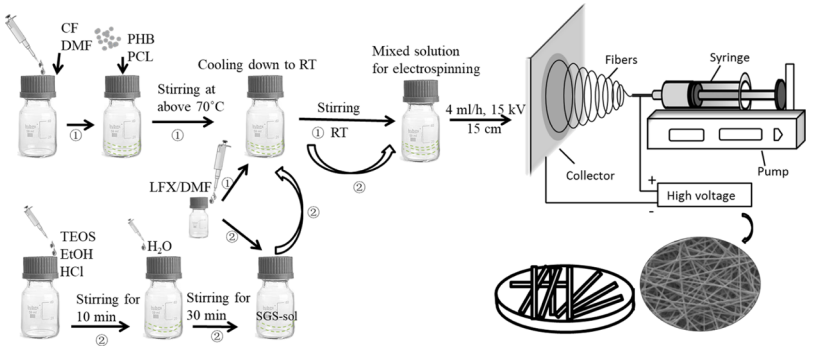

Figure 1. Schematic illustration of the preparation procedures of P100L5 (route 1) and P100S20L5 (route 2) electrospun fibermats.

positive bacteria.[13] In the present study, LFX was used as a model drug to be incorporated into SGS-containing scaffolds to further eliminate the potential infection after operation. It is considered that drug incorporation may influence the morphology and physical performance of the nanocomposites and hybrids. Moreover, drug release behavior may also vary when in contact with hybrid systems. Their morphologies and physical properties of scaffolds with and without LFX were compared in detail, and their drug release profiles and antibacterial efficacy against Gram-positive bacteria *Staphylococcus aureus* (*S. aureus*) and Gram-negative bacteria *Escherichia coli* (*E. coli*) were investigated. Furthermore, MG-63 osteoblast-like cell cultivation was carried on the above LFX-containing scaffolds to evaluate their biological performances.

2. MATERIALS AND METHODS

2.1. Materials. PHB (M_w = 437 kDa) and PCL (M_w = 48−90 kDa) were dissolved in chloroform (CF) and *N*,*N*-dimethylformamide (DMF) to prepare the polymer solution. For silica sol preparation, tetraethyl orthosilicate (TEOS, 98%), ethanol (EtOH, 99.5%), hydrogen chloride (HCl, 1 N), and DI H_2O were used as a precursor, a solvent, and a catalyst. LFX (≥98.0%) was utilized as a model drug to examine the antibacterial properties. All chemicals were commercially purchased from Sigma-Aldrich.

2.2. Fabrication of PHB/PCL/SGS/LFX Fibermats. For a comparative study, PHB/PCL/LFX fibermats were first prepared. As illustrated in Figure 1, 0.35 g of PHB and 0.15 g of PCL were dissolved in a cosolvent consisting of 8 mL of CF and 1 mL of DMF at 70 °C under intense magnetic stirring. In addition, 25 mg of LFX was dissolved in 1 mL of DMF at room temperature. Afterward, the LFX solution was added dropwise into the PHB/PCL solution until a homogeneous solution was obtained for electrospinning at room temperature (Figure 1, route 1). The weight ratio of LFX in comparison to polymer matrix was 1:20, and the sample was labeled as P100L5.

To fabricate the sol−gel silica (SGS)-containing sample, a two-step procedure was involved. First, 9 mL of PHB (0.35 g)/PCL (0.15 g)-CF (8 mL)/DMF (1 mL) solution and 1 mL of LFX (25 mg)−DMF solution were prepared through the same process as described above. At the same time, 0.93 mL of TEOS was dissolved in 0.485 mL of EtOH until clear and then 0.15 mL of H_2O and 4 μL of HCl (1 N) were dropped into the TEOS solution and stirred for 30 min to prepare the silica sol. Then, 1 mL of LFX−DMF solution was mixed with 628 μL of as-prepared silica sol until a homogeneous mixture was obtained and further added into the PHB/PCL−CF/DMF solution for electrospinning (Figure 1, route 2). The polymer/SGS and polymer/LFX ratios were fixed at 5:1 and 20:1, respectively; thus, the sample was labeled as P100S20L5.

All mixtures were electrospun following the flow rate of 4 mL/h and an electric field of 15 kV/15 cm for 2.5 h to obtain fiber meshes with thicknesses around 100−150 μm. An aluminum foil was used as a collector for final scaffolds. All processes were conducted at room temperature, and the humidity was kept at 30−40%. For comparison, pure PHB/PCL fibermats were also fabricated using the same concentration and operational parameters. Afterward, all samples were dried in a vacuum oven for 24 h before further characterizations.

2.3. Physicochemical Characterizations. *2.3.1. Morphology.* The morphologies of as-prepared samples were observed by scanning electron microscopy (SEM, Ultra Plus, Zeiss, Germany). In addition, fiber diameter distributions were measured by ImageJ through SEM images, and more than 100 fibers were chosen randomly for each image. All samples were sputter-coated with gold/palladium before observation.

2.3.2. Tensile Property. The mechanical properties were evaluated by a tensile testing machine (Frank, Karl Frank GmbH, Germany) on rectangular strip samples with a size of 40 × 5 mm^2. Stress−strain curves were recorded when the samples were stretched at a speed of 10 mm/min by the testXpert program (Zwick/Roell, Germany) using a load cell of 50 N. The ultimate tensile strength, strain at break, and elastic modulus were determined from the stress−strain curves, and average values were calculated on five samples.

2.3.3. Wettability. The wettability was testified by contact angle (CA) measurements (DSA30, Kruess GmbH, Germany). During each measurement, a water droplet of 6 μL was dropped onto the sample and five measurements were conducted on each composition.

2.3.4. Fourier Transform Infrared Spectroscopy. Attenuated total reflectance Fourier transform infrared spectroscopy (ATR−FTIR, Nicolet 6700, Thermo Scientific, USA) was utilized to investigate the chemical structure of the obtained samples. For each measurement, 32 spectral scans were repeated in the wavenumber range of 4000−525 cm^{-1}.

2.4. In Vitro Drug Release Studies. All samples were cut into strips with dimensions of 40 × 5 mm^2, and the total drug content was calculated as a function of sample weight and designed weight ratio. Then, the drug release behavior was tested by immersing two types of samples in 20 mL of phosphate-buffered saline (PBS) solution at 37 °C. At each time point, 1 mL of the immersing PBS was extracted for testing and 1 mL of fresh PBS was refilled. The absorbance of UV light of the 1 mL extracted PBS solution was measured with a UV−vis spectrophotometer (SPECORD 40, Analytik Jena, Germany) at 288 nm. Afterward, the concentration was interpreted through an absorbance−concentration calibration curve ranging from 5 to 100 μg/mL. Curves of cumulative release over time were plotted. The experiments were conducted in triplicates.

2.5. Antibacterial Studies. The antibacterial performance of obtained sample was tested against both Gram-positive bacteria *S. aureus* and Gram-negative bacteria *E. coli*. First, the above microorganisms were precultured in Luria−Bertani Broth (LB medium, Carl Roth GmbH, Karlsruhe, Germany) overnight in a shaker at 37 °C. Then, the bacterial pellets were collected and dispersed in the sterilized LB medium, and the bacterial density was standardized by an OD_{600} to an optical density of 0.01. Briefly, to assess the inhibitory activity of as-prepared samples against bacterial, 20 μL of *S. aureus* diluted suspension or *E. coli* suspension was uniformly spread onto respective agar plates and then square samples with a size of 5 × 5 mm^2 were placed onto the above agar plates and incubated for 24 h at

DOI: 10.1021/acsami.8b02656
ACS Appl. Mater. Interfaces 2018, 10, 14540−14548

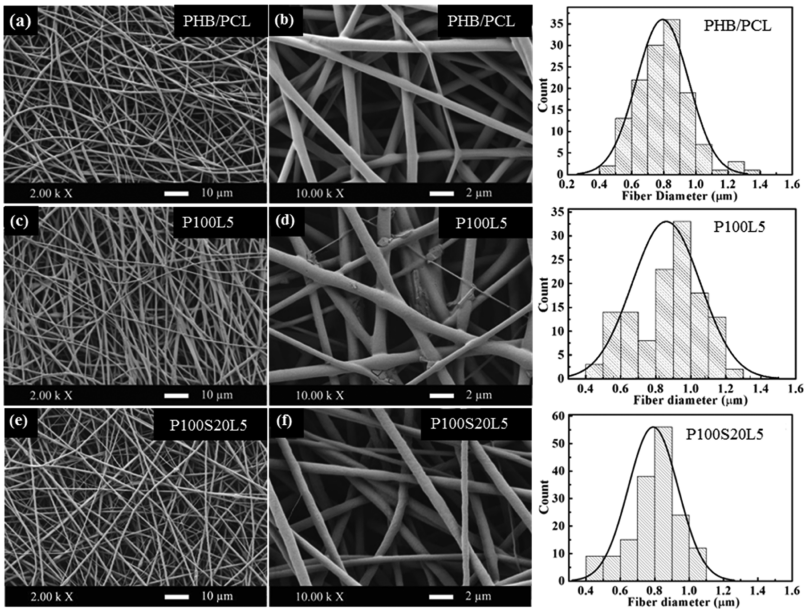

Figure 2. SEM images and fiber diameter distributions of PHB/PCL (a,b), P100L5 (c,d), and P100S20L5 (e,f).

37 °C. Subsequently, the zone of inhibition around the samples on the agar plates was visually inspected.

2.6. In Vitro Cellular Behavior. MG-63 osteoblast-like cells (Sigma-Aldrich, USA) were cultured in a Dulbecco's modified Eagle's medium (HyClone, Logan, UT) with 4.5 g/L glucose, supplemented with 10% fetal bovine serum (Gibco, Invitrogen, USA), 1% nonessential amino acids, 1% L-glutamine, penicillin (100 IU/mL), and streptomycin (100 μg/mL) (all from HyClone, Logan, UT). The cells were cultured under a 95% humidified atmosphere with 5% CO_2 at 37 °C. The medium was changed every other day. As-prepared samples were cut into pieces at a size of 5 × 5 mm^2 and then inserted onto the bottom of the culture plates, followed by sterilization under UV light.

2.6.1. Cytotoxicity. To investigate the cytotoxicity of the prepared scaffolds, MG-63 cells were seeded onto the samples in 96-well plates at a density of 1 × 10^4 cells per well and alamarBlue Cell Viability Assay (Thermo Fisher Scientific, USA) was utilized. After cell culture for 1 and 3 days, the culture medium was removed and samples were incubated in a fresh Hanks' balanced salt solution containing 10 vol % alamarBlue solutions at 37 °C in 5% CO_2 for another 4 h. When the medium color changed from blue to light pink, the luminescence of the reacted medium (100 μL) was measured using a Varioskan Flash plate reader (Thermo Fisher Scientific, USA), which proportionally indicated the live cell numbers. The experiments were repeated in triplicates.

2.6.2. Cell Adhesion and Morphology. MG-63 cells were seeded onto the samples in 48-well plates at a density of 2 × 10^4 cells per well and then cultivated in the medium for 3 and 7 days. At each time point, the samples were fixed with 4% paraformaldehyde for 10 min and then washed with PBS three times. Before observation by confocal laser scanning microscopy (Leica TCS SP5 II HCS A, Germany), the cells were permeabilized with 0.1% Triton X-100 for 5 min, rinsed with PBS, and blocked with 1% bovine serum albumin solution for 20 min. After that, the cytoskeletons were stained with Alexa Fluor 488 phalloidin for 20 min and nuclei were stained using 4′,6-diamidino-2-phenylindole (DAPI) for 5 min.

To observe the cell morphologies by SEM, MG-63 cells were cultured onto the samples in 48-well plates at a density of 2 × 10^4 cells per well for 3 and 7 days. At each time point, cell-seeded samples were fixed in 2.5% glutaraldehyde for 30 min, rinsed with PBS several times, and then dehydrated through concentration-graded ethanol at 30, 50, 70, 80, 90, and 100% for 15 min each. The dehydrated samples were sputter-coated with platinum before SEM observation (Quanta 250 FEG, FEI, USA).

2.6.3. Cell Alkaline Phosphatase Activity. The alkaline phosphate activity (ALP) is regarded as an initial indicator of the osteoblast phenotype.[14] An ALP assay kit (Fluorometric, Abcam, UK) was used to measure the ALP activity according to the manufacturer's instructions. In brief, after cell cultivation for 7 and 14 days, a supernatant of cell lysate was collected to react with the non-fluorescent 4-methylumbelliferone phosphatase disodium salt (MUP) substrate in 96-well black plates with clear bottoms. The plates were subsequently incubated at room temperature in the dark for 30 min. During the incubation, the substrate MUP was dephosphorylated to the fluorescent chemical by active ALP obtained in the cell lysate. Emission of the fluorescent substrate was measured at 440 nm using Varioskan Flash plate reader (Thermo Fisher Scientific, USA). A standard curve was generated each time, and the results were normalized to the control sample (PHB/PCL at day 7, 100%).

2.6.4. Quantitative Assessment of Alizarin Red S Staining for Mineralization. Mineralization of cells on the substrate is another sign of osteogenic differentiation of relevance to bone tissue engineering.[14,15] Alizarin Red S (ARS) staining was used to detect the presence of calcified calcium nodules on the scaffolds and MG-63 cells, which were cultured on the scaffolds at a density of 5 × 10^3 cells per well for 4 weeks. After the cell culture, all samples were rinsed with PBS and fixed with 95% ethanol for 10 min. Afterward, they were immersed in ARS staining solution (pH = 4.2) for 10 min to stain the calcium, followed by H_2O rinsing to remove excess dye. Then, the ARS uptake in calcium minerals was extracted by using a 10% acetic acid for 30 min. Finally, the mineralization content was quantified by determining the optical density of extracted ARS using the Varioskan Flash plate reader (Thermo Fisher Scientific, USA). The obtained values were then normalized to the control sample (PHB/PCL at day 28, 100%).

2.7. Statistical Analysis. All data were expressed as average ± standard deviation (SD). A one-way analysis of variance followed by the Bonferroni post hoc test was used to analyze the data. The analysis was carried out using OriginPro 9.0 software (OriginLab Corporation, USA), and the levels of significance were set at the probabilities of $*p < 0.05$, $**p < 0.01$, and $***p < 0.001$.

3. RESULTS AND DISCUSSION

3.1. Morphologies of Scaffolds. To facilitate cell growth and proliferation, a 3D structure with interconnected pores is desired to closely mimic the ECM, which is the microenvironment supporting the cellular activities and metabolism.[16] As shown in Figure 2, all three samples exhibit smooth, nonwoven,

DOI: 10.1021/acsami.8b02656
ACS Appl. Mater. Interfaces 2018, 10, 14540−14548

Table 1. Fiber Diameter Distributions, Tensile Properties, and Wettabilities (CA Values) for PHB/PCL, P100L5, and P100S20L5 (The Data Are Mean Value ± Standard Deviation, $n \geq 5$)

	diameter (μm)	ultimate tensile strength (MPa)	strain at failure (%)	Young's modulus (MPa)	CA (deg)	CA (deg) at 20 min
PHB/PCL	0.8 ± 0.2	3.5 ± 0.1	195 ± 31	98 ± 10	137 ± 5	135 ± 3
P100L5	0.9 ± 0.2	4.0 ± 0.3	175 ± 23	153 ± 9	122 ± 4	0
P100S20L5	0.8 ± 0.1	2.4 ± 0.1	50 ± 4	122 ± 8	135 ± 2	0

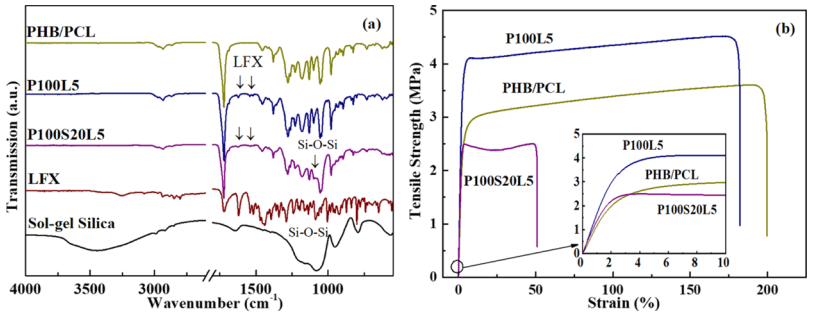

Figure 3. (a) FTIR spectra of PHB/PCL, P100L5, and P100S20L5. (b) Representative stress−strain curves of PHB/PCL, P100L5, and P100S20L5 samples in tensile strength tests (n = 5).

and highly porous architecture, which is the typical topography of optimized electrospun fibermats. Moreover, the fiber diameters of all samples display a comparable distribution range (Figure 2 and Table 1), indicating that the LFX addition had no significant influence on the spinnability of the solution. The topographies of the LFX-containing scaffolds differed in terms of fiber surfaces. Compared to pure polymer scaffolds, drug crystal-like particles appear on the fiber surfaces of P100L5 (Figure 2d), whereas P100S20L5 exhibits smooth and uniform fiber surfaces (Figure 2f).

Particles on the P100L5 samples (Figure 2d) may be drug crystals, as drug crystal formation and growth were often reported in electrospun hydrophobic fibers containing hydrophilic drugs and were assumed to be caused mainly by the incompatibility between the polymers and drugs.[17] In addition, several parameters were especially investigated on the drug crystal formation by Zeng et al.[18] They proposed that solubility and compatibility in the polymer/drug/solvent system were the decisive factors influencing drug distribution and crystal formation, and the hydrophilic (drug)−hydrophobic (polymer) relationship could highly induce the drug crystallization on the fiber surface. The above study can reasonably explain the drug crystal-like aggregates in scaffolds consisting of hydrophobic PHB/PCL matrix and hydrophilic LFX incorporation. However, in the P100S20L5 system, the high solubility of LFX in acid silica sol (pH ≈ 4) and the better compatibility between LFX and silanol moieties (−Si−OH) were assumed to inhibit the crystalline LFX formation. It was reported that the solubility of LFX in water is pH-dependent and reaches a maximum of 200 mg/mL when the pH ranges from 2 to 5.[19] Additionally, according to Radin et al.'s study, SGS xerogels were able to entrap hydrophilic drug (vancomycin) in the network as a drug carrier.[20] Thus, it is likely that LFX was completely dissolved in the mixture and confined in the silica network during electrospinning, resulting in smooth fiber generation without drug aggregates. The formation and distribution of drug crystals could influence the physical properties and the release profiles, as discussed below.

3.2. Chemical Structure. The chemical structures evidenced by FTIR spectra of the as-prepared scaffolds are presented in Figure 3a to verify the inclusion of SGS and LFX. As the FTIR spectra of PHB, PCL, and SGS have been thoroughly discussed in the previous study,[11,12] only drug related information will be discussed here. Most bands of LFX are overlapping with those of the polymers; however, two bands at 1621 and 1540 cm^{-1} can characteristically prove the incorporation of LFX.[21] In addition, the presence of SGS can also be confirmed by the band area in the range of 1200−1000 cm^{-1}.[11] No apparent new bands or band shift can be detected because of the overlapping and low amount of LFX addition.

3.3. Mechanical Performances. Besides the topography, matrix stiffness is also reported to strongly affect cellular behavior. For instance, more proliferative and spreading cell phenotype could be observed on a stiffer matrix.[22,23] Thus, the mechanical properties were evaluated on LFX-containing samples to examine the influence of drug incorporation. Representative stress−strain curves are displayed in Figure 3b, and a summary of the average values is listed in Table 1. As shown in stress−strain curves, the ductile fracture feature of the PHB/PCL blend is maintained for all LFX-containing samples. Tensile strength and Young's modulus of P100L5 were highly increased due to LFX addition. This is likely due to the formation of drug crystals which reinforced the polymer matrix in a manner similar to rigid nanoparticles.[24] Similar results were reported in the studies of electrospun cellulose acetate fibers containing gallic acid and electrospun PCLEEP fibers encapsulated with retinoic acid.[24,25] Furthermore, in the P100S20L5 system containing both SGS and LFX, despite the decreased tensile strength and strain, Young's modulus was also increased ~24% compared to that of the pure PHB/PCL scaffolds. In our former study, SGS-alone inclusion could enhance the strength and stiffness of pure PHB/PCL fibermats simultaneously.[11] On the contrary, the LFX incorporation into SGS may interfere with the sol−gel network formation, leading to the reduction of the tensile strength.

3.4. Wettability. Surface wettability (hydrophilicity−hydrophobicity) of scaffolds is considered as one of the most essential factors affecting biological responses, such as initial cellular adhesion and proliferation behaviors, protein adhesion, and bacterial adhesion.[26,27] Moreover, in drug release systems, the permeation rate of water and the drug diffusion rate are both related to the hydrophilicity.[28] Therefore, in addition to

DOI: 10.1021/acsami.8b02656
ACS Appl. Mater. Interfaces 2018, 10, 14540−14548

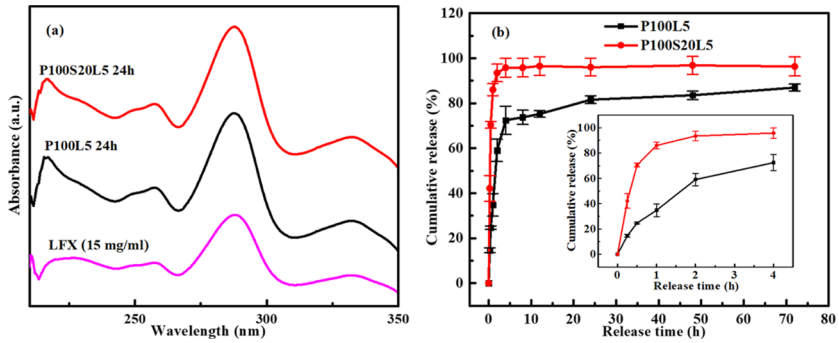

Figure 4. (a) UV−vis spectra of pure LFX/PBS and released LFX/PBS from electrospun P100L5 and P100S20L5 samples after 24 h. (b) Cumulative release of LFX from the samples P100L5 and P100S20L5 up to 72 h (n = 3).

physical performance, the wettability of the scaffolds was assessed by measuring the CAs and the results are summarized in Table 1. As the data shows, all LFX-containing samples were very hydrophobic after fabrication and at the initial stage of measurement, which can be attributed to the hydrophobic nature of PHB and PCL and the high porosity of electrospun structures.[29] However, unlike pure PHB/PCL scaffolds, the CAs of the LFX-containing samples decreased to 0° after 20 min, which was evidenced by the fact that water drops were absorbed into the scaffolds gradually during the measurement. It is proven that the hydrophilic LFX on the fiber surface dramatically changed the wettability of the fibrous scaffolds. Additionally, the SGS addition could also increase the hydrophilicity of hybrid scaffolds according to our previous study;[11] therefore, both SGS and LFX contributed to the hydrophilicity of the current hybrid PHB/PCL/SGS/LFX scaffolds. Similar trends were observed in a study about electrospun collagen/PCL scaffolds containing penicillin and tetracycline.[28]

3.5. Drug Release Behavior. As drug carrier and delivery systems, electrospun scaffolds can achieve a high drug loading and encapsulation efficiency. Moreover, the drug release kinetics can be modulated through altering the composition and structure of the fibers.[30] To investigate the release behaviors of LFX in the present systems, a 72 h release study was carried out in PBS solutions. Figure 4a shows the UV−vis spectra of pure LFX and the released LFX from electrospun scaffolds, and cumulative release profiles of the two LFX-containing scaffolds are shown in Figure 4b. From the UV−vis measurement, it is observed that the released LFX from all scaffolds for 24 h displays the same curves to that of pure LFX. All spectra show the maximum absorbance peaks at 288 nm, which indicates that the integrity of the LFX molecule was preserved during the whole procedure, including the sol−gel process and the electrospinning process. From the cumulative release profiles, it can be seen that all scaffolds show a quick burst release of LFX in the first 8 h, followed by a sustained release up to 72 h. However, the initial amount of LFX released after 8 h is a function of the scaffold composition. Comparatively, nearly 74 wt % of LFX was released from pure PHB/PCL in the first 8 h, and almost 95 wt % of LFX was released from SGS-containing scaffolds. The initial accelerating release of LFX from P100S20L5 can be clearly compared in the inset in Figure 4b. In addition, the total amount of LFX released from P100L5 after 72 h is 87 wt %, and this value almost reaches 96.7 wt % for P100S20L5, implying accelerated LFX release due to SGS addition.

Intrinsically, the drug release rate from electrospun scaffolds can be controlled by the degradation of the polymer matrix and the interactions between drug and matrix.[31] In our early studies,[32] the hydrolytic degradation of PHB/PCL was quite slow (less than 5% in PBS for up to 12 months) and thus, it will not significantly contribute to the LFX release in our systems. Thus, the incompatibility of the hydrophilic drug (LFX) in the hydrophobic polymer (PHB/PCL) and the high ionic strength of the drug molecule and the rapid solvent evaporation during electrospinning, all contribute to the LFX molecules tending to be located near the surface of the electrospun fibers and thus be dissolved easily in the medium, leading to the rapid burst release profile.[33,34] The highly increased LFX release in SGS-containing samples can be mainly attributed to the fast dissolution of the silica phase.[35] Similar conclusions were drawn from a study on PCL/sol−gel silica/tetracycline system with varying silica contents (0−20 vol %).[36]

3.6. Antibacterial Activity. The bacterial inhibitory activity of as-prepared scaffolds was evaluated by the agar diffusion test using Gram-positive bacteria *S. aureus* and Gram-negative bacteria *E. coli*. As indicated in Figure 5, the efficacy of the incorporated LFX was evaluated by measuring the inhibition zone. It was observed that both P100L5 and P100S20L5 scaffolds are able to effectively inhibit the bacterial growth under the studied conditions, and the inhibition zones

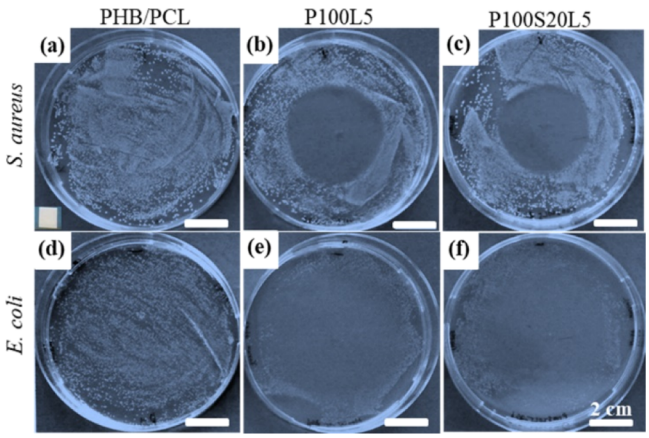

Figure 5. Antibacterial tests against Gram-positive bacterial *S. aureus* and Gram-negative bacterial *E. coli* after culturing on agar plates with electrospun samples of PHB/PCL (a,d), P100L5 (b,e), and P100S20L5 (c,f) for 24 h. The diameter of inhibition zone in (b) is 44 ± 3 and 43 ± 2 mm in (c). The size of samples was 5 × 5 mm^2, and an example of the testing sample was in the left corner of (a).

DOI: 10.1021/acsami.8b02656
ACS Appl. Mater. Interfaces 2018, 10, 14540−14548

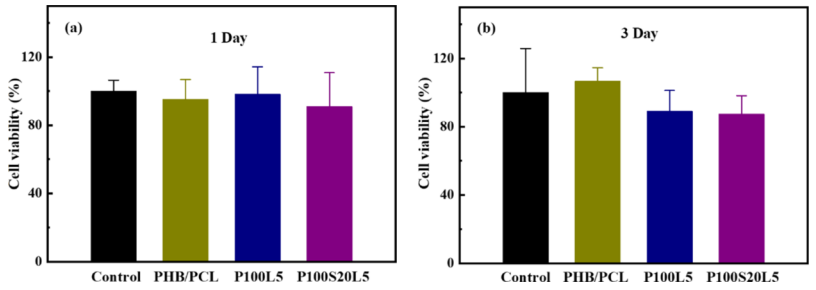

Figure 6. Cell viability of MG-63 cells when cultivated in fibrous scaffolds for 1 (a) and 3 days (b); the tissue culture plate was used as the control (the results were presented as average value ± SD, n = 3).

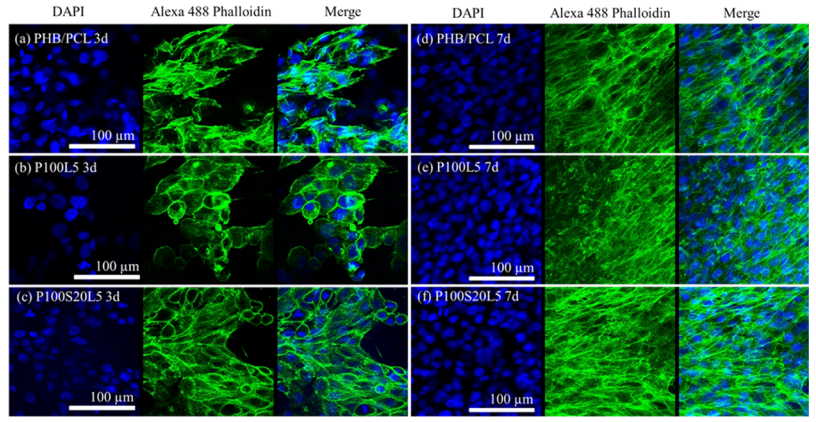

Figure 7. Confocal images of MG-63 cells when cultivated on scaffolds PHB/PCL (a,d), P100L5 (b,e), and P100S20L5 (c,f) for 3 and 7 days (same scale bar for all images).

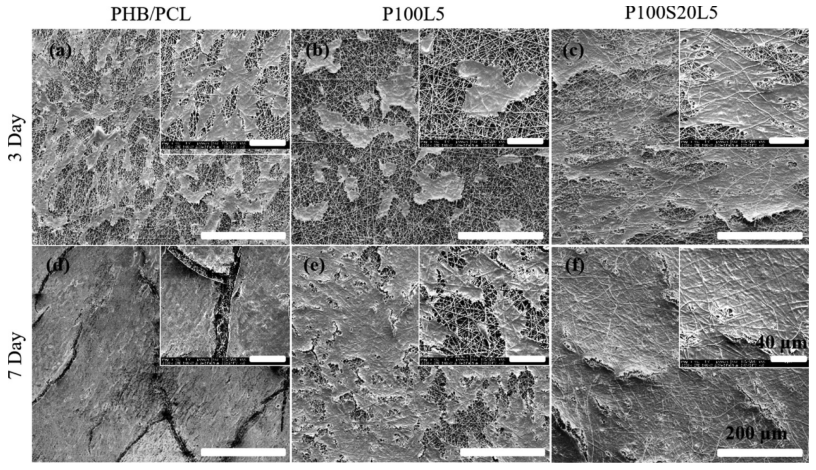

Figure 8. SEM images of MG-63 cells when cultivated on the scaffolds PHB/PCL (a,d), P100L5(b,e), and P100S20L5 (c,f) for 3 and 7 days. (The scale bar is 200 μm; the scale bar of the inset is 40 μm).

of the two LFX-containing scaffolds against *S. aureus* after 24 h are basically similar in diameter, which is 44 ± 3 mm for P100L5 and 43 ± 2 mm for P100S20L5, implying that the drug release patterns did not significantly affect the antibacterial efficacy. As shown in Figure 5d–f, for LFX-containing samples, most of the bacterial colonies disappeared and only few of the colonies can be seen around the boundary of the culture plate after culturing for 24 h against *E. coli*, suggesting that the released LFX has a stronger inhibitory effect on *E. coli* bacteria in comparison to *S. aureus* bacteria. No significant differences were observed between the efficacy of P100L5 and P100S20L5 against *E. coli*.

3.7. In Vitro Cellular Behavior. A systematic biological study was conducted on the LFX-containing samples to evaluate the influence of LFX inclusion on biocompatibilities.

3.7.1. Cell Viability. A high dose of antibiotics might significantly interfere with cell replication and even cause cell death.[37,38] Therefore, it is important to understand whether the loaded LFX in P100L5 and P100S20L5 causes cytotoxicity. The cytotoxicity was evaluated using the alamarBlue cell viability assay after cell cultivation for 1 and 3 days. As shown in Figure 6a, all scaffolds exhibited comparable cell viability to the control (tissue culture plate) after cell culture for 1 day. Although the values were slightly lower when cells were cultivated in P100L5 and P100S20L5 for 3 days (Figure 6b), the results among all

DOI: 10.1021/acsami.8b02656
ACS Appl. Mater. Interfaces 2018, 10, 14540–14548

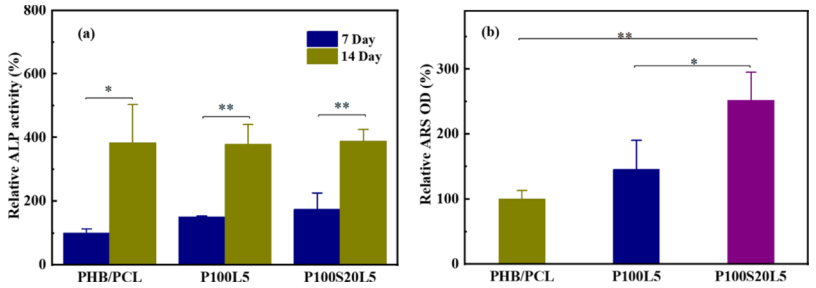

Figure 9. (a) ALP activity of MG-63 cells when cultured on PHB/PCL, P100L5, and P100S20L5 scaffolds for 7 and 14 days, and ALP activity of PHB/PCL scaffolds after cell culture for 7 days was used as a control. (b) Uptake of ARS by the calcified minerals when cultured PHB/PCL, P100L5, and P100S20L5 scaffolds in the presence of MG-63 cells for 28 days, and the ARS value of PHB/PCL scaffolds was used as a control. (The results were presented as average value ± SD, n = 3).

samples have no significant differences. Thus, LFX in our systems has no significant cytotoxicity on the MG-63 cells.

3.7.2. Cell Adhesion and Morphology. Confocal microscopy was utilized to visualize the cellular adhesion and morphologies when cells were cultivated for 3 and 7 days on the fibrous scaffolds. As demonstrated in Figure 7a–c, cell numbers after cultivation for 3 days on LFX-containing samples were slightly less when compared to the results on pure PHB/PCL scaffolds, which is consistent with the cell viability results in Figure 6b. In addition, the cell skeleton stained by phalloidin shows a relatively round or ellipsoid shape on sample P100L5, whereas typical spindle-shape cells were found on PHB/PCL and SGS-containing scaffolds P100S20L5. This distinction indicated that the addition of LFX restrained cell adhesion and growth in the early stages of cell culture, and this negative influence can be reduced by silica addition to some extent. The confocal images after cell culture for 7 days (Figure 7d–f) verified that bipolar MG-63 cells fully covered all three samples, indicating that LFX inclusion has no severe inhibitory effect on the cell growth and migration behaviors.

Furthermore, cell–scaffold interactions were further investigated by SEM (Figure 8). After cell culture for 3 days, cells on PHB/PCL and P100S20L5 exhibited comparable cellular proliferation and elongated spindle-like morphologies. On the other hand, cells on P100L5 appeared spherical and more separated from each other. After culture for 7 days, cells on all samples formed a homogeneous cell layer, consistent with the confocal images discussed above. However, cells on LFX-containing samples (P100L5 and P100S20L5) displayed closer attachment to the substrate than pure PHB/PCL scaffolds, which can be attributed to the significantly enhanced hydrophilicity of LFX-containing samples (Table 1).

3.7.3. ALP Activity and Mineralization. ALP activity is the primary index to assess the differentiation of osteoblast cells.[14,15] As demonstrated in Figure 9a, all samples showed significantly increased ALP activity after 14 days when compared to cell culture for 7 days. However, there is no significant difference among the three samples at each culture period, suggesting that LFX addition has no negative influence on the osteogenicity of osteoblast-like cells in our study.

After cell culture for 28 days, ARS was used to stain the mineral nodules and calcium depositions to evaluate the mineralization content of scaffolds in the presence of MG-63 cells, which is proportionally related to the optical density of ARS staining extraction. As indicated in Figure 9b, although there is no significant difference between the ARS values of P100L5 and PHB/PCL, P100S20L5 showed a significantly enhanced content of mineralization compared to P100L5 and PHB/PCL, suggesting that the SGS addition could favorably promote the mineralization activity. This result is consistent with the study of Kim et al., regarding the effects of silicon on osteoblast activity.[15] Their research revealed that the effect of ALP activity of osteoblasts was directly dependent on silicon-ion concentration and only a medium high dose of silicon ions could favorably promote the ALP activity. Instead, the mineralization content showed a constant increase when silicon ions concentration ranged from 0 to 100 mM.[15]

Overall, electrospinning showed to be a versatile technique to integrate multiple functions especially for tissue engineering. The current study concentrates on the development of a drug carrier capability for organic/inorganic hybrid fibermats. Results indicated that the solubility and compatibility changed when LFX was included into the PHB/PCL/SGS hybrid system, leading to a distinct influence on the physicochemical performances and drug release behavior. The biocompatibility and antibacterial function of LFX-containing samples were verified, and the potential to facilitate osteodifferentiation and mineralization of osteoblasts was confirmed on SGS-containing scaffolds, making the hybrid system a prospective option for tissue engineering applications.

4. CONCLUSIONS

LFX was incorporated into PHB/PCL and PHB/PCL/SGS hybrid scaffolds to achieve antibacterial function. Morphology observations indicated that LFX drug crystal-like particles appeared on the PHB/PCL fiber surface. Scaffolds containing both LFX and SGS exhibited a smooth surface without particles. With regard to mechanical performance, 5 wt % of LFX inclusion can greatly reinforce the pure polymer matrix. However, this enhancement effect was compromised when SGS was added to the system. Moreover, LFX addition can reverse the hydrophobicity of PHB/PCL scaffolds. Release profiles of LFX from both scaffolds exhibited a biphasic release behavior consisting of an initial burst release and followed by a sustained release. Nevertheless, the scaffolds containing both SGS and LFX showed an accelerated release of LFX compared to LFX-alone scaffolds. Two types of scaffolds showed comparable antibacterial efficacy against both Gram-positive and Gram-negative bacteria (*S. aureus* and *E. coli*). All scaffolds were nontoxic to MG-63 osteoblast-like cells. Comparable cell adhesion and growth behaviors were observed after cell culture for 7 days. Although the osteodifferentiation behavior evidenced by ALP activity after cell cultivation for 14 days shows no significant difference among the scaffolds, the amount of mineralization nodules after cell culturing for 28 days on scaffolds PHB/PCL/SGS/LFX was significantly higher than

DOI: 10.1021/acsami.8b02656
ACS Appl. Mater. Interfaces 2018, 10, 14540–14548

that of pure PHB/PCL and PHB/PCL/LFX scaffolds because of the silica phase dissolution. Overall, the electrospun biocompatible and antibacterial scaffolds containing both LFX and SGS are promising for bone tissue engineering applications.

AUTHOR INFORMATION

Corresponding Authors

*E-mail: helder.santos@helsinki.fi (H.A.S.).
*E-mail: judith.roether@fau.de (J.A.R.).

ORCID

Wei Li: 0000-0002-6997-9611
Kai Zheng: 0000-0002-2573-6677
Dongfei Liu: 0000-0002-2426-134X
Aldo R. Boccaccini: 0000-0002-7377-2955
Hélder A. Santos: 0000-0001-7850-6309

Notes

The authors declare no competing financial interest.

ACKNOWLEDGMENTS

Y.D. would like to acknowledge the China Scholarship Council for financial support. H.A.S. acknowledges financial support from the University of Helsinki Research Funds, the Sigrid Juselius Foundation (grant no. 4704580), the HiLIFE Research Funds, and the European Research Council under the European Union's Seventh Framework Programme (FP/2007-2013; grant no. 310892). The authors acknowledge the following core facilities funded by Biocenter Finland: Electron Microscopy Unit of the University of Helsinki for providing the facilities for TEM imaging.

REFERENCES

(1) Thenmozhi, S.; Dharmaraj, N.; Kadirvelu, K.; Kim, H. Y. Electrospun nanofibers: New Generation Materials for Advanced Applications. *J. Mater. Sci. Eng. B* **2017**, *217*, 36−48.
(2) Hu, X.; Liu, S.; Zhou, G.; Huang, Y.; Xie, Z.; Jing, X. Electrospinning of Polymeric Nanofibers for Drug Delivery Applications. *J. Controlled Release* **2014**, *185*, 12−21.
(3) Thakkar, S.; Misra, M. Electrospun Polymeric Nanofibers: New Horizons in Drug Delivery. *Eur. J. Pharm. Sci.* **2017**, *107*, 148−167.
(4) Khorshidi, S.; Solouk, A.; Mirzadeh, H.; Mazinani, S.; Lagaron, J. M.; Sharifi, S.; Ramakrishna, S. A Review of Key Challenges of Electrospun Scaffolds for Tissue-Engineering Applications. *J. Tissue Eng. Regener. Med.* **2016**, *10*, 715−738.
(5) Zamani, M.; Prabhakaran, M. P.; Ramakrishna, S. Advances in Drug Delivery via Electrospun and Electrosprayed Nanomaterials. *Int. J. Nanomed.* **2013**, *8*, 2997−3017.
(6) Hadjiargyrou, M.; Chiu, J. B. Enhanced Composite Electrospun Nanofiber Scaffolds for Use in Drug Delivery. *Expert Opin. Drug Delivery* **2008**, *5*, 1093−1106.
(7) Di Martino, A.; Liverani, L.; Rainer, A.; Salvatore, G.; Trombetta, M.; Denaro, V. Electrospun Scaffolds for Bone Tissue Engineering. *Musculoskelet. Surg.* **2011**, *95*, 69−80.
(8) Li, W.; Wang, H.; Ding, Y.; Scheithauer, E. C.; Goudouri, O.-M.; Grünewald, A.; Detsch, R.; Agarwal, S.; Boccaccini, A. R. Antibacterial 45S5 Bioglass®-based Scaffolds Reinforced with Genipin Cross-linked Gelatin for Bone Tissue Engineering. *J. Mater. Chem. B* **2015**, *3*, 3367−3378.
(9) Li, W.; Ding, Y.; Rai, R.; Roether, J. A.; Schubert, D. W.; Boccaccini, A. R. Preparation and Characterization of PHBV Microsphere/45S5 Bioactive Glass Composite Scaffolds with Vancomycin Releasing Function. *Mater. Sci. Eng. C.* **2014**, *41*, 320−328.
(10) Choi, J. S.; Kim, H. S.; Yoo, H. S. Electrospinning Strategies of Drug-incorporated Nanofibrous Mats for Wound Recovery. *Drug Delivery Transl. Res.* **2015**, *5*, 137−145.
(11) Ding, Y.; Roether, J. A.; Boccaccini, A. R.; Schubert, D. W. Fabrication of Electrospun Poly (3-hydroxybutyrate)/Poly (ε-caprolactone)/Silica Hybrid Fibermats with and without Calcium Addition. *Eur. Polym. J.* **2014**, *55*, 222−234.
(12) Ding, Y.; Yao, Q.; Li, W.; Schubert, D. W.; Boccaccini, A. R.; Roether, J. A. The Evaluation of Physical Properties and *in vitro* Cell Behavior of PHB/PCL/sol−gel Derived Silica Hybrid Scaffolds and PHB/PCL/Fumed Silica Composite Scaffolds. *Colloids Surf., B* **2015**, *136*, 93−98.
(13) Noel, G. J. A Review of Levofloxacin for the Treatment of Bacterial Infections. *Clin. Med. Ther.* **2009**, *1*, CMT.S28.
(14) Golub, E. E.; Boesze-Battaglia, K. The Role of Alkaline Phosphatase in Mineralization. *Curr. Opin. Orthop.* **2007**, *18*, 444−448.
(15) Kim, E.-J.; Bu, S.-Y.; Sung, M.-K.; Choi, M.-K. Effects of Silicon on Osteoblast Activity and Bone Mineralization of MC3T3-E1 Cells. *Biol. Trace Elem. Res.* **2013**, *152*, 105−112.
(16) Curry, A. S.; Pensa, N. W.; Barlow, A. M.; Bellis, S. L. Taking Cues from the Extracellular Matrix to Design Bone-mimetic Regenerative Scaffolds. *Matrix Biol.* **2016**, *52*−*54*, 397−412.
(17) Gao, Y.; Truong, Y. B.; Zhu, Y.; Kyratzis, I. L. Electrospun Antibacterial Nanofibers: Production, Activity, and in vivo Applications. *J. Appl. Polym. Sci.* **2014**, *131*, 40797.
(18) Seif, S.; Franzen, L.; Windbergs, M. Overcoming Drug Crystallization in Electrospun Fibers—Elucidating Key parameters and Developing Strategies for Drug Delivery. *Int. J. Pharm.* **2015**, *478*, 390−397.
(19) Frick, A.; Möller, H.; Wirbitzki, E. Biopharmaceutical Characterization of Oral Immediate Release Drug Products. In vitro/in vivo Comparison of Phenoxymethylpenicillin Potassium, Glimepiride and Levofloxacin. *Eur. J. Pharm. Biopharm.* **1998**, *46*, 305−311.
(20) Radin, S.; Ducheyne, P.; Kamplain, T.; Tan, B. H. Silica Sol-gel for the Controlled Release of Antibiotics. I. Synthesis, Characterization, and in vitro Release. *J. Biomed. Mater. Res. A.* **2001**, *57*, 313−320.
(21) Shahwal, V. K.; Dubey, B. K.; Bhoumick, M. Preformulation Study of Levofloxacin. *Int. J. Adv. Pharm.* **2012**, *1* (1), 1−8.
(22) Wells, R. G. The Role of Matrix Stiffness in Regulating Cell Behavior. *Hepatology* **2008**, *47*, 1394−1400.
(23) Chen, G.; Dong, C.; Yang, L.; Lv, Y. 3D Scaffolds with Different Stiffness but the Same Microstructure for Bone Tissue Engineering. *ACS Appl. Mater. Interfaces* **2015**, *7*, 15790−15802.
(24) Chew, S. Y.; Hufnagel, T. C.; Lim, C. T.; Leong, K. W. Mechanical Properties of Single Electrospun Drug-encapsulated Nanofibres. *Nanotechnology* **2006**, *17*, 3880−3891.
(25) Phiriyawirut, M.; Phaechamud, T. Gallic Acid-loaded Cellulose Acetate Electrospun Nanofibers: Thermal Properties, Mechanical Properties, and Drug Release Behavior. *Open J. Polym. Chem.* **2012**, *02*, 21−29.
(26) Xu, L.-C.; Siedlecki, C. A. Effects of Surface Wettability and Contact Time on Protein Adhesion to Biomaterial Surfaces. *Biomaterials* **2007**, *28*, 3273−3283.
(27) Papenburg, B. J.; Rodrigues, E. D.; Wessling, M.; Stamatialis, D. Insights into the Role of Material Surface Topography and Wettability on Cell-material Interactions. *Soft Matter* **2010**, *6*, 4377−4388.
(28) Prabu, P.; Kim, K. W.; Dharmaraj, N.; Park, J. H.; Khil, M. S.; Kim, H. Y. Antimicrobial Drug Release Scaffolds of Natural and Synthetic Biodegradable Polymers. *Macromol. Res.* **2008**, *16*, 303−307.
(29) Nuraje, N.; Khan, W. S.; Lei, Y.; Ceylan, M.; Asmatulu, R. Superhydrophobic Electrospun Nanofibers. *J. Mater. Chem. A* **2013**, *1*, 1929−1946.
(30) Chou, S.-F.; Carson, D.; Woodrow, K. A. Current Strategies for Sustaining Drug Release from Electrospun Nanofibers. *J. Controlled Release* **2015**, *220*, 584−591.
(31) Kouhi, M.; Morshed, M.; Varshosaz, J.; Fathi, M. H. Poly (ε-caprolactone) Incorporated Bioactive Glass Nanoparticles and simvastatin Nanocomposite Nanofibers: Preparation, Characterization and in vitro Drug Release for Bone Regeneration Applications. *Chem. Eng. J.* **2013**, *228*, 1057−1065.

DOI: 10.1021/acsami.8b02656
ACS Appl. Mater. Interfaces 2018, 10, 14540−14548

(32) Ding, Y. Development of Electrospun Poly-3-hydroxybutyrate-based Composite and Hybrid Scaffolds for Bone Tissue Engineering. Ph.D. Thesis, Friedrich-Alexander-Universität Erlangen−Nürnberg, Erlangen, Germany, 2015.
(33) Kim, K.; Luu, Y. K.; Chang, C.; Fang, D.; Hsiao, B. S.; Chu, B.; Hadjiargyrou, M. Incorporation and Controlled Release of a Hydrophilic Antibiotic using Poly (lactide-co-glycolide)-based Electrospun Nanofibrous Scaffolds. *J. Controlled Release* **2004**, *98*, 47−56.
(34) Haroosh, H. J.; Dong, Y.; Ingram, G. D. Synthesis, Morphological Structures, and Material Characterization of Electrospun PLA: PCL/Magnetic Nanoparticle Composites for Drug Delivery. *J. Polym. Sci., Part B: Polym. Phys.* **2013**, *51*, 1607−1617.
(35) Kortesuo, P.; Ahola, M.; Karlsson, S.; Kangasniemi, I.; Yli-Urpo, A.; Kiesvaara, J. Silica Xerogel as an Implantable Carrier for Controlled Drug Delivery—Evaluation of Drug Distribution and Tissue Effects after Implantation. *Biomaterials* **2000**, *21*, 193−198.
(36) Shin, K.-H.; Koh, Y.-H.; Kim, H.-E. Synthesis and Characterization of Drug-Loaded Poly(-caprolactone)/Silica Hybrid Nanofibrous Scaffolds. *J. Nanomater.* **2013**, *2013*, 351810.
(37) Miclau, T.; Edin, M. L.; Lester, G. E.; Lindsey, R. W.; Dahners, L. E. Effect of Ciprofloxacin on the Proliferation of Osteoblast-like MG-63 Human Osteosarcoma Cells in vitro. *J. Orthop. Res.* **1998**, *16*, 509−512.
(38) Duewelhenke, N.; Krut, O.; Eysel, P. Influence on Mitochondria and Cytotoxicity of Different Antibiotics Administered in High Concentrations on Primary Human Osteoblasts and Cell Lines. *Antimicrob. Agents Chemother.* **2007**, *51*, 54−63.

DOI: 10.1021/acsami.8b02656
ACS Appl. Mater. Interfaces 2018, 10, 14540−14548